An Interior Observer's Holonomic Cosmology

Richard S. Phillips *

Posted Date: 26 March 2026

doi: 10.20944/preprints202602.1803.v2

Keywords: Lorentz holonomy; tetrad formalism; Einstein–Dirac solitons; compton wavelength; timescape cosmology; holographic screens; differential geometry

 doi:10.20944/preprints202602.1803.v2

Article

An Interior Observer's Holonomic Cosmology

Richard S. Phillips

Information Physics Institute, Gosport, UK; richard.s.phillips@informationphysicsinstitute.net

Abstract

General relativity and quantum field theory divide the world into geometry and matter. We develop a framework in which the Lorentz symmetry shared by both theories provides a basis for challenging this duality: the bivector generators that govern spinor propagation in the Dirac equation simultaneously govern how spacetime frames compose in the tetrad formulation of general relativity. When the spin connection acquires nontrivial holonomy in a compact conjugacy class, boost–rotation noncommutativity ($[K_i, K_j] = -\epsilon_{ijk} J_k$) implies that the configuration cycles internally at a rate set by the confinement scale, suggesting an identification of the Compton frequency with geometric confinement. Explicit Einstein–Dirac solitons illustrate this mechanism: a massless five-dimensional spinor acquires mass $m_n = |n|\hbar/(cR_0)$ from a discrete topological sector, with no mass parameter in the fundamental Lagrangian. Within this framework, observers built from wound geometry would be unable to access their absolute gravitational depth—only derivatives and ratios of $\ln a$. The physically meaningful content of those ratios can be packaged covariantly: a depth functional $\mathcal{N}(\tau)$ built from holographic-screen areas is strictly monotone by the Bousso–Engelhardt area theorem, and its projection onto void and wall congruences yields $C(a) = \sqrt{A_w/A_v}$—a quantity structurally analogous to the lapse-drift variable in Wiltshire's timescape cosmology—suggesting a reinterpretation of cosmic acceleration as an interior-calibration effect within unmodified general relativity.

Keywords: Lorentz holonomy; tetrad formalism; Einstein–Dirac solitons; compton wavelength; timescape cosmology; holographic screens; differential geometry

---

1. Introduction

The universe appears to be accelerating. Type Ia supernova data, confirmed independently by BAO measurements and the CMB, show that distant objects are receding faster than a matter-dominated expansion would predict. The standard explanation is a cosmological constant—a uniform energy density filling empty space, whose observed value is roughly 10^{-120} times the natural quantum-gravitational scale. No first-principles derivation of this value exists.

An alternative explanation, developed quantitatively over eighteen years by Wiltshire's timescape program [14,15], is that the acceleration is apparent. The universe is not homogeneous: bound structures—galaxies, clusters, walls of the cosmic web—sit at greater gravitational depth than expanding voids, and this depth separation increases as new structures virialize. From the deep side, looking outward, the expansion of the void is measured with clocks that run slow and rulers that are compressed; the result looks like acceleration. From the void side, the same structures are simply settling deeper into their wells while the void passively dilates. Neither description is preferred; both are projections of a single, growing depth gradient. Timescape fits supernovae [16], accommodates BAO and CMB acoustic scales [17], and has received recent support from numerical-relativity void statistics [18]—all without a cosmological constant.

But timescape is incomplete. It describes the lapse drift between void and wall congruences but does not derive it from first principles. It lacks a covariant formulation of its central variable. And it has no microphysical account of *why* matter produces the kind of curvature that generates a sign-definite, cumulative depth separation—as opposed to a fluctuating one that averages away.

 doi:10.20944/preprints202602.1803.v2

This paper proposes to address all three gaps by tracing them to an algebraic structure that general relativity and quantum field theory already share but interpret differently. The six generators of the Lorentz group appear in both theories: in the Dirac equation, as the Clifford bivectors $\sigma^{ab} = \frac{1}{4}[\gamma^a, \gamma^b]$ governing spinor propagation; in the tetrad formulation of general relativity, as the local boost and rotation content of the gravitational field. These are the same generators satisfying the same commutation relations in the same representation. Quantum field theory uses the anticommutator structure to propagate a particle *through* a fixed geometry; general relativity uses the commutator structure to describe how geometry itself is oriented at each point. In the standard metric formulation, the six Lorentz degrees of freedom carried by the tetrad are absorbed into $g_{\mu\nu}$ and treated as gauge—a choice that is correct when spacetime topology is trivial.

But the Lorentz group itself contains compact rotational subgroups—SO(3), or SU(2) in the spin representation—whose closed orbits admit periodic structure. When curvature is present, the spin connection acquires nontrivial holonomy: a net Lorentz transformation accumulated around a closed path whose conjugacy class is gauge-invariant and cannot be smoothly reduced to the identity. If that holonomy lies in a compact (elliptic) conjugacy class, the configuration cycles internally in proper time. The algebraic mechanism is the commutation relation $[K_i, K_j] = -\epsilon_{ijk} J_k$: boosts in different directions generate rotations, providing an intrinsic loop-closure that is a structural property of the algebra, not an external imposition. The tighter such a configuration is confined, the faster it cycles. The cycling rate is the Compton frequency $\omega_C = mc^2/\hbar$; the confinement scale is the Compton wavelength $\lambda_C = h/(mc)$; in this reading, mass is the eigenvalue of geometric confinement.

Two preceding papers [3,4] developed this identification using the mathematical apparatus of string theory—winding numbers, T-duality, Calabi–Yau structure—without physical strings, and demonstrated quantitative particle-physics predictions. The present paper embeds it into classical general relativity by constructing explicit, finite-energy solutions of the coupled Einstein–Dirac system that realize nontrivial holonomy sectors as dynamically self-consistent solitons. The minimal realization uses a single compact spatial cycle S^1 of circumference $2\pi R_0$; a massless five-dimensional spinor acquires four-dimensional mass $m_n = |n|\hbar/(cR_0)$ from the discrete winding number n, with no mass parameter in the fundamental Lagrangian. The winding sources the lapse well that confines it, and the solutions satisfy the null energy condition required by the cosmological construction that follows.

If matter is wound geometry, then every measuring instrument an observer builds—rulers, clocks, atomic transition frequencies—is wound from the same geometry whose depth it is trying to measure. A ruler that participates in conformal rescaling cannot detect its own rescaling—the same principle illustrated by Ehrenfest's spinning disk [5], where instruments welded to the geometry contract with it and register no change. The absolute gravitational depth—the value of the lapse α at a single point—is therefore operationally hidden; only the spatial gradient $\nabla \ln \alpha$ (gravity), temporal drift $\partial_t \ln \alpha$ (expansion), and ratios of proper-time accumulation between worldlines are accessible from within.

The cosmological consequence is sign-definite because virialization is irreversible: once a region has collapsed and converted its expansion budget into intrinsic spatial curvature via the Hamiltonian constraint, the depth separation persists. The depth continues to grow even after local equilibration, because depth and curvature are not the same thing—curvature has an asymptotic limit set by the geometry of the source, while the relational depth between two causal horizons grows for as long as proper time elapses and null rays continue to be focused. We define a covariant depth functional $\mathcal{N}(\tau) = \frac{1}{2} \ln\big(A[\sigma(\tau)]/4\pi\ell_P^2\big)$ from the maximal-area cuts of an observer's past light cone, whose strict monotonicity follows from the Bousso–Engelhardt area theorem [27,28] under the null energy condition. Its cosmological projection onto void and wall congruences yields $C(a) = \sqrt{A_w/A_v}$—a screen-area ratio structurally analogous to the lapse-drift variable in Wiltshire's timescape program [14,15], now grounded in the four-dimensional geometry rather than postulated.

The logical chain of the paper runs in the direction opposite to this introduction: from the Lorentz algebra, through the tetrad and holonomy, to topological confinement as mass, the conformal ruler,

 doi:10.20944/preprints202602.1803.v2

the covariant depth functional, and finally the cosmological lapse drift. Section 2 begins that chain by showing how general relativity encodes the gravitational field as a compression of local frames—a boost structure visible in the Schwarzschild and Painlevé–Gullstrand metrics and spanning all six Lorentz degrees of freedom in the Kerr geometry.

2. The Holonomic Platform

2.1. Two Ways to See Curvature

The Schwarzschild metric encodes the compression structure described in the Introduction [5,6]:

$$ds^2 = -\left(1 - \frac{r_s}{r}\right)c^2\,dt^2 + \left(1 - \frac{r_s}{r}\right)^{-1} dr^2 + r^2\,d\Omega^2\,, \tag{2.1}$$

where $r_s = 2GM/c^2$. The factor $(1 - r_s/r)$ is a compression factor: it governs how much local clocks slow and local rulers contract relative to a distant reference. At $r = r_s$, the factor vanishes—the horizon, a property of geometry under sufficient compression, not of exotic matter.

But the Schwarzschild metric hides something. Its coordinate singularity at $r = r_s$ is an artifact of the time coordinate, not of the geometry. Painlevé [10] showed in 1921 that the same geometry can be rewritten by replacing the Schwarzschild time with the proper time of freely falling observers:

$$ds^2 \;=\; -c^2\,d\tau_{\rm ff}^2 + \left(dr + c\sqrt{\frac{r_s}{r}}\,d\tau_{\rm ff}\right)^2 + r^2\,d\Omega^2\,. \tag{2.2}$$

Read this line by line. The spatial part is flat: $dr^2 + r^2\,d\Omega^2$ is Euclidean three-space. What has changed is the relationship between radial position and time: the $dr\,d\tau_{\rm ff}$ cross-term says that holding a fixed spatial position requires fighting an inward drift at velocity $v(r) = -c\sqrt{r_s/r}$. The geometry has not changed—it is still the Schwarzschild solution—but in these coordinates, curvature does not appear as a static deformation of space. It appears as a *flow*: space itself moves radially inward, carrying local inertial frames along with it.

Hamilton and Lisle [9] developed this into the river model of black holes. In their picture, a freely falling observer is simply carried along by the current of space; a hovering observer must swim upstream. At the horizon, the flow reaches the speed of light—no upstream swimming is possible. The compression factor $(1 - r_s/r)$ and the infall velocity $v = -c\sqrt{r_s/r}$ are two descriptions of the same geometric content, but the river picture reveals something the Schwarzschild form conceals: the local reference frame at each point is *boosted* relative to the asymptotic frame, tilted in the time-radial plane by the infall.

For the non-rotating (Schwarzschild) case, this tilt is purely radial—a boost. But for a rotating (Kerr) black hole, the flow acquires a second component: frame dragging [9]. Space does not merely fall inward; it also *twists* azimuthally around the spin axis. The local frame is now simultaneously boosted by the infall and rotated by the dragging. The boost has three independent components (one per spatial axis); the rotation has three independent components (one per plane of rotation). Together, these six—three boosts K_i and three rotations J_i—span a six-dimensional algebra, and the gravitational field of a Kerr black hole uses all six at every point.

This is not a peculiarity of black holes. These six components—three boosts and three rotations forming the Lorentz algebra $\mathfrak{so}(1,3)$—are present in general relativity at every spacetime point, for every geometry. The Schwarzschild metric hides them by absorbing the boost into a time-time coefficient; the Painlevé–Gullstrand form reveals the boost as a flow; the Kerr solution activates the full algebra. The passage from tetrad to metric discards all six as gauge. But in a geometry with nontrivial topology—where the flow can wind, close on itself, and persist—they become the physical degrees of freedom. To see them, we need the formalism that tracks them explicitly.

 doi:10.20944/preprints202602.1803.v2

2.2. The Lorentz Algebra Inside General Relativity

Conventions.

Latin indices $a, b, \ldots$ label Lorentz/tetrad components; Greek indices $\mu, \nu, \ldots$ label spacetime tensor components. The curvature 2-form $R^{ab} = d\omega^{ab} + \omega^a{}_c \wedge \omega^{cb}$ corresponds to the Riemann tensor $R^\rho{}_{\sigma\mu\nu}$; null focusing is governed by the Ricci contraction $R_{\mu\nu}k^\mu k^\nu$.

The tetrad (vierbein) $e^a{}_\mu$ is a set of four orthonormal basis vectors at each spacetime point, with sixteen components. The metric is a derived object:

$$g_{\mu\nu} \;=\; \eta_{ab}\, e^a{}_\mu\, e^b{}_\nu \,. \tag{2.3}$$

This equation is invariant under local Lorentz transformations—rotations and boosts of the basis vectors—which remove six of the sixteen components, leaving the ten independent metric degrees of freedom. In topologically trivial settings, these six are pure gauge. But they are the same six that the river model reveals as the physical content of the gravitational field: the boosts and rotations that describe how local frames are tilted relative to the asymptotic frame. In a time-gauge tetrad adapted to a chosen observer congruence, $e^0{}_0 = \alpha$ coincides with the ADM lapse.

The spin connection ω^{ab} is the gauge field of this Lorentz structure—a 1-form on spacetime taking values in $\mathfrak{so}(1,3)$, the six-dimensional algebra spanned by J_i and K_i [6,8]. The curvature 2-form

$$R^{ab} \;=\; d\omega^{ab} + \omega^a{}_c \wedge \omega^{cb} \tag{2.4}$$

is its field strength. Einstein gravity is the dynamics of this $\mathfrak{so}(1,3)$-valued gauge field; the metric is its shadow, capturing the curvature but discarding the internal Lorentz structure that the river model made visible.

2.3. Trivial Topology: Why Einstein Was Right

In the topologically trivial sector—vacuum, no winding, no persistent structure—local frame orientation is genuinely redundant. Boosting or rotating your tetrad at a point cycles you through the curvature decomposition at that point: electric-type tidal components map into magnetic-type frame-dragging components and back. But the metric $g_{\mu\nu} = \eta_{ab}\, e^a{}_\mu\, e^b{}_\nu$ is invariant under this rotation, so the curvature profile it encodes does not change. The electric and magnetic components reshuffle; their geometric content does not. That is what makes the six a gauge freedom in this sector.

Einstein was right to remove these six degrees of freedom for classical vacuum physics. What follows addresses the regime where he was not required to.

2.4. Nontrivial Topology: When Gauge Becomes Physical

A gauge symmetry says: local transformations are undetectable. But topology can obstruct the "local" part of that statement.

Transport a local Lorentz frame around a closed path in spacetime using the spin connection ω^{ab}. When the frame returns to its starting point, it may have undergone a net rotation or boost: the *holonomy*

$$\mathrm{Hol}_\gamma(\omega) \;=\; \mathcal{P} \exp \oint_\gamma \omega \;\in\; \mathrm{SO}(1,3)\,, \tag{2.5}$$

where $\mathcal{P}$ denotes path ordering. Under local Lorentz gauge transformations, the holonomy conjugates: $\mathrm{Hol}_\gamma \mapsto \Lambda\, \mathrm{Hol}_\gamma\, \Lambda^{-1}$, so only its conjugacy class is gauge-invariant; nontrivial topology prevents reduction to the identity class.

The holonomy is the physical content of a winding. It is to the Lorentz connection what the Aharonov–Bohm phase is to the electromagnetic potential: locally pure gauge, globally observable.

 doi:10.20944/preprints202602.1803.v2

2.5. Two Readings of One Algebra

The generators σ^{ab} of $\mathfrak{so}(1,3)$ in the Dirac representation,

$$\sigma^{ab} \;=\; \tfrac{1}{4}[\gamma^a,\,\gamma^b]\,, \tag{2.6}$$

participate in two algebraic structures simultaneously.

The *anticommutator* structure defines the Clifford algebra $\mathrm{Cl}(1,3)$:

$$\{\gamma^a,\,\gamma^b\} \;=\; 2\,\eta^{ab}\,\mathbf{1}\,. \tag{2.7}$$

This defines the tangent-space inner product: the flat Minkowski signature η^{ab} that determines which directions are timelike and which are spacelike at each point. The gamma matrices act on a four-component spinor ψ; the Dirac equation $(i\gamma^\mu\partial_\mu - m)\psi = 0$ describes the spinor's propagation through a fixed spacetime background. In this reading, geometry is the stage; the spinor is the actor.

The *commutator* structure defines the Lie algebra $\mathfrak{so}(1,3)$:

$$[\sigma^{ab},\,\sigma^{cd}] \;=\; \eta^{bc}\sigma^{ad} - \eta^{ac}\sigma^{bd} - \eta^{bd}\sigma^{ac} + \eta^{ad}\sigma^{bc}\,. \tag{2.8}$$

This governs how Lorentz transformations compose. In the holonomic reading, the same commutator structure governs how boosts and rotations of the geometry itself compose and close into loops [3]. There is no separate object being acted upon. The geometry winds, and in the holonomic reading the winding *is* the particle.

Both structures live in the same algebra. The Clifford reading uses the anticommutator to propagate an object through geometry; the holonomic reading uses the commutator to wind geometry into an object. Neither reading is more fundamental; they are two projections of one algebraic fact.

A remark on the logical status of this identification is appropriate. The standard framework assumes that matter fields are independent entities propagating on a geometric background—that the spinor ψ and the connection ω^{ab} are ontologically distinct objects that happen to share the same $\mathfrak{so}(1,3)$ algebra. But this assumption has no mathematical derivation; it is a historical default inherited from the division of labor between general relativity and quantum field theory. Once one observes that the Lorentz algebra's commutator structure generates topologically closed configurations (Appendix B), and that those configurations can self-consistently source the geometry that confines them (Section 4), there is no mathematical reason to postulate a separate, non-geometric substance to fill that role. The holonomic reading does not add structure to general relativity; it declines to subtract structure that the tetrad formulation already contains. Whether this reading is physically correct is an empirical question, addressed in part by the cosmological construction of Sections 5–7. But the burden of proof is symmetric: the assumption that matter is independent of geometry is no more derived than the proposal that it is not.

2.6. The Explicit Map

The six independent components of σ^{ab} decompose as

$$\underbrace{\sigma^{12},\;\sigma^{23},\;\sigma^{31}}_{J_i\ \text{(rotations)}} \qquad \underbrace{\sigma^{01},\;\sigma^{02},\;\sigma^{03}}_{K_i\ \text{(boosts)}}, \tag{2.9}$$

where each spatial axis $\hat{x}_i$ contributes one rotation generator $J_i = \epsilon_{ijk}\sigma^{jk}$ (embedding oscillation in the plane perpendicular to $\hat{x}_i$) and one boost generator $K_i = \sigma^{0i}$ (embedding oscillation coupling $\hat{x}_i$ to the time direction).

In Ref. [3], particle states are modeled as stable oscillatory modes of spacetime geometry—confined winding configurations on a compact T^6 manifold whose topology prevents smooth deformation to the vacuum sector. That construction assigns to each macroscopic spatial axis a bisecting plane with two

 doi:10.20944/preprints202602.1803.v2

independent transverse oscillatory directions $(\hat{u}_i, \hat{v}_i)$, yielding $3 \times 2 = 6$ Lorentz degrees of freedom that close pairwise into loops under commutation. These map directly:

$$\hat{u}_i \leftrightarrow J_i\,, \qquad \hat{v}_i \leftrightarrow K_i\,. \tag{2.10}$$

The identification is not an interpretive choice; it is forced by the fact that both constructions span the same six-dimensional algebra with the same commutation relations. The loop closure used in Ref. [3] to build winding configurations is Baker–Campbell–Hausdorff composition of finite Lorentz transformations—the exponential map of $\mathfrak{so}(1,3)$.

The detailed construction of the winding states—how these generators close into loops, how three orthogonal bisecting planes assemble into a $T^2 \times T^2 \times T^2$ topology, and how the resulting winding numbers map to observed particle quantum numbers—is developed in [3]. Appendix B derives the algebraic mechanism: boost–rotation noncommutativity generates closed holonomy loops, nontrivial topology makes them topologically stable, and compact elliptic holonomy implies a proper-time phase rate identified with mass. Section 4 constructs explicit self-consistent solutions of the coupled Einstein–Dirac system realizing these winding sectors as finite-energy solitons. What we require in the main text is the consequence: *stable confined oscillatory configurations of the Lorentz structure exist, and their confinement scale determines their mass.*

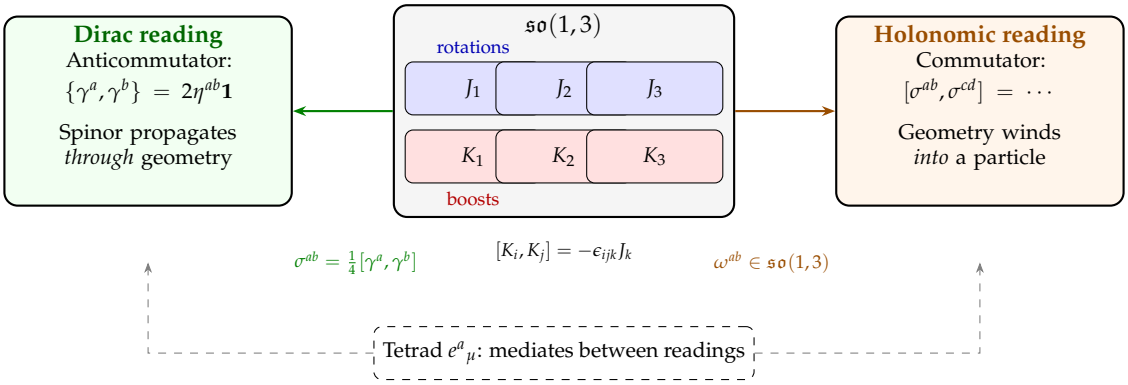

Figure 1. The six generators of $\mathfrak{so}(1,3)$ participate in two algebraic structures simultaneously. The Dirac reading (left) uses the anticommutator to propagate a spinor through geometry; the holonomic reading (right) uses the commutator to wind geometry into a particle. The tetrad $e^a{}_\mu$ mediates between the two readings.

3. From Winding to Mass

3.1. The Tetrad as Mediator

The tetrad $e^a{}_\mu$ introduced in Section 2.2 determines which algebraic reading applies. Its departure from $\delta^a{}_\mu$ *is* the local tilt of the Lorentz bivectors relative to the coordinate frame—the same tilt the river model made visible as spatial flow.

In a region of topologically trivial geometry—flat spacetime, weak-field perturbations—the tetrad can be gauged to $\delta^a{}_\mu$ everywhere. The Lorentz structure is aligned; nothing winds. Spinors propagate through this background, and the Dirac reading is the natural description.

In a region of nontrivial winding, the tetrad is nontrivial: the local frame is boosted and rotated relative to the asymptotic frame. This tilt produces two things simultaneously: the curvature that *defines* the winding ($R^{ab} \neq 0$ because the connection has nontrivial holonomy), and the clock-rate variation that *measures* its depth. In the holonomic reading, "winding" refers to nontrivial holonomy of the Lorentz connection; its stress-energy cost is what appears as $T_{\mu\nu}$ in Einstein's equation. The time-time projection of the tetrad,

$$e^0{}_0 = \alpha\,, \tag{3.1}$$

is the ADM lapse function $\alpha = d\tau/dt$—the ratio of proper time to coordinate time. This is the master observable of the rest of this paper.

 doi:10.20944/preprints202602.1803.v2

3.2. Self-Animation

If a particle is a topological configuration, what gives it dynamics?

The coincidence of the gauge degrees of freedom with the curvature decomposition is not a redundancy to be discarded—it is the mechanism of internal oscillation. At any point inside a winding, the local Lorentz structure has both boost-like and rotation-like components. Boosting through the curvature at that point cycles the decomposition: electric-type (tidal stretching) maps into magnetic-type (frame dragging) and back. In a topologically closed configuration, this cycling has nowhere to terminate; it is periodic. The winding does not need an external clock or driving force; existing as a closed Lorentz configuration and cycling through that configuration are the same thing.

In the holonomic framework we identify the internal cycling rate with the observed Compton frequency,

$$\omega_C = \frac{mc^2}{\hbar}. \tag{3.2}$$

Tighter confinement means the loop closes on a shorter scale, the cycling completes faster, and the frequency is higher. The Compton wavelength

$$\lambda_C = \frac{h}{mc} \tag{3.3}$$

measures the spatial scale of the confinement. In this framework, mass is not a substance deposited into geometry; it is the degree of geometric confinement.

3.3. The Core Identity

A particle confined to scale λ_C draws the surrounding geometry inward—not by exerting a force, but because the winding *is* a region where space has been pulled into a tighter configuration. This drawing-in is curvature. Curvature produces a gradient in the clock rate: $\nabla \ln \alpha \neq 0$ in the neighborhood of the winding. The energy cost of the confinement, measured by a distant clock, is mass.

These are not five sequential steps in a causal chain; within the holonomic framework, they are mathematically equivalent descriptions of the same geometric configuration:

Tighter confinement = more space drawn in = curvature = clock-rate gradient = mass

The Einstein field equations $G_{\mu\nu} = (8\pi G/c^4)\, T_{\mu\nu}$ are, in this reading, the self-consistency condition for geometry that can confine itself. The left-hand side describes the curvature; the right-hand side describes the energy cost of the confinement. In this reading, they represent two consistent descriptions of the same geometric configuration. Since every particle is a winding of the same $\mathfrak{so}(1,3)$-valued connection on the same manifold, every winding responds identically to a clock-rate gradient—offering a natural account of the equivalence principle.

4. Self-Consistent Winding Configurations

Sections 2–3 argued that the Lorentz algebra supports topologically stable winding configurations whose confinement scale determines mass, and Appendix B derives the algebraic mechanism. This section demonstrates that the claim is dynamically self-consistent: the coupled Einstein–Dirac system admits localized, finite-energy solutions in which no mass parameter is introduced in the fundamental Lagrangian—mass emerges as the eigenvalue of a nonlinear boundary-value problem in which the winding sources the lapse well that confines it. The only mass scale entering the effective four-dimensional equations is fixed by a topological sector label and the scale of a compact direction. These solutions satisfy the null energy condition required for the screen-area monotonicity of Section 6.2.

 doi:10.20944/preprints202602.1803.v2

4.1. Assumptions and Scope

The construction rests on four assumptions consistent with the rest of this paper. (i) The connection is torsion-free (Levi-Civita); no independent torsion degrees of freedom are introduced. (ii) A compact direction exists; the minimal case treated here is a single circle S^1; the full $T^2 \times T^2 \times T^2$ extension of Refs. [3,4] is deferred. (iii) The static, spherically symmetric sector is used as the minimal constructive existence witness. (iv) A two-spinor singlet construction is employed so that the combined stress-energy tensor is spherically symmetric [30].

This section supplies a mathematical existence witness: explicit solutions of the Einstein field equations satisfying the stated energy conditions. Self-consistent determination of the compactification scale (radion stabilization) is identified as an open problem in Section 7.3.

4.2. Minimal Topological Realization

In torsion-free general relativity, the spin connection ω^{ab} is uniquely determined by the metric through the metricity condition; it carries no independent degrees of freedom in four dimensions. A strictly massless Dirac field in asymptotically flat 3+1 spacetime is conformally invariant and admits no normalizable bound states. A mass scale must therefore enter through topology, not through the Lagrangian.

The minimal realization uses one non-contractible spatial cycle S^1 of circumference $2\pi R_0$—the simplest representative of the compact sector of Refs. [3,4]. A massless higher-dimensional spinor field $\Psi(x^\mu, \chi)$ on $\mathcal{M}^4 \times S^1$ carries a discrete mode number $n \in \mathbb{Z}$ around the cycle:

$$\Psi(x^\mu, \chi) = e^{in\chi}\, \psi_n(x^\mu)\,. \tag{4.1}$$

The covariant derivative along the compact direction produces an effective four-dimensional mass:

$$\boxed{m_n = \frac{|n|\hbar}{c\, R_0}}\,. \tag{4.2}$$

No free mass parameter appears in the five-dimensional Lagrangian; the only inputs are the topological sector label n and the geometric cycle scale R_0.

The sector label n admits a dual interpretation: as Kaluza–Klein momentum, it is the quantized eigenvalue of the compact-direction derivative; as a holonomy label, it classifies the conjugacy class of the spin bundle's monodromy around S^1. In the notation of Appendix B, n is the winding number of the Lorentz holonomy restricted to the compact cycle. Both descriptions yield the same effective mass (4.2) and the same reduced field equations.

The compactification radius R_0 is treated here as a geometric datum. Promoting it to a dynamical radion field $R(r)$ whose stabilization at a self-consistent value R_* converts m_n from a parameter into a prediction; this upgrade is identified as an open problem in Section 7.3.

 doi:10.20944/preprints202602.1803.v2

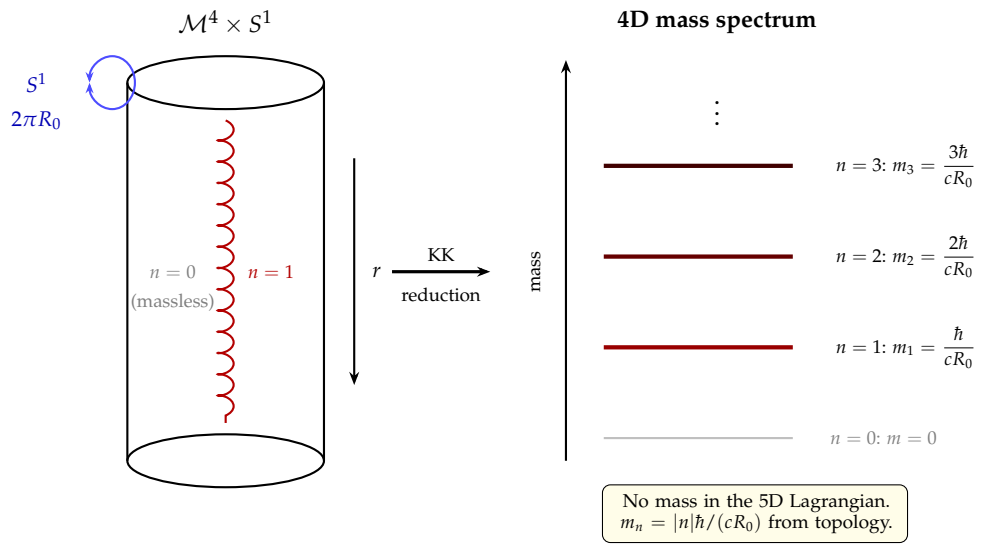

Figure 2. Kaluza–Klein mass generation. A massless five-dimensional spinor on $\mathcal{M}^4 \times S^1$ acquires a discrete four-dimensional mass spectrum $m_n = |n|\hbar/(cR_0)$ from the winding number n around the compact cycle. No mass parameter appears in the fundamental Lagrangian.

4.3. The Coupled Einstein–Dirac System

Integrating the massless five-dimensional action over S^1 yields a four-dimensional Einstein–Dirac system with effective mass m_n. We work in the static, spherically symmetric sector. Following the conventions of Ref. [30], this subsection adopts signature $(+,-,-,-)$; all invariant quantities and the physical lapse $\alpha = 1/T$ are independent of this choice.

Metric.

In Schwarzschild gauge, with a notation chosen to avoid collision with the screen area $A[\sigma]$ of Section 6.2:

$$ds_4^2 = \frac{1}{T(r)^2}\,dt^2 \;-\; \frac{1}{B(r)}\,dr^2 \;-\; r^2\,d\Omega^2\,, \tag{4.3}$$

where $B(r) = 1 - 2m(r)/r$ defines the mass function $m(r)$ and the physical lapse is $\alpha(r) = 1/T(r)$ (cf. Equation (3.1)).

Spin connection.

The torsion-free spin connection determined by (4.3) has boost component $\omega^{01} \propto (T'/T)\sqrt{B}$, sourced by the lapse gradient, and rotation components $\omega^{12}, \omega^{13} \propto \sqrt{B}$, sourced by spatial curvature. Both are activated simultaneously in any localized configuration; this is the concrete realization of the boost–rotation cycling $[K_i, K_j] = -\epsilon_{ijk}J_k$ described in Section 3.2 and derived algebraically in Appendix B.

Dirac ansatz.

A time-harmonic mode with energy eigenvalue E (we use E for the spectral parameter, reserving ω for the spin connection) takes the form

$$\psi(t,r,\theta,\varphi) = e^{-iEt}\,\frac{1}{r}\begin{pmatrix} \Phi_1(r)\,\Omega_{\kappa m}(\theta,\varphi) \\ i\,\Phi_2(r)\,\Omega_{-\kappa m}(\theta,\varphi) \end{pmatrix}, \tag{4.4}$$

where $\Omega_{\kappa m}$ are spin-spherical harmonics with $\kappa = \pm(j + \frac{1}{2})$. The two-spinor singlet construction ensures spherically symmetric $T_{\mu\nu}$ [30].

 doi:10.20944/preprints202602.1803.v2

The closed ODE system.

Substituting (4.3) and (4.4) into the coupled Einstein–Dirac equations yields, in natural units $c = \hbar = G = 1$:

$$\boxed{\begin{aligned}
\sqrt{B}\,\Phi_1' &= \frac{\kappa}{r}\,\Phi_1 \;-\; \big(E\,T + m_n\big)\,\Phi_2\,, \\
\sqrt{B}\,\Phi_2' &= \big(E\,T - m_n\big)\,\Phi_1 \;-\; \frac{\kappa}{r}\,\Phi_2\,, \\
r\,B' &= 1 - B \;-\; 16\pi\,E\,T^2\big(\Phi_1^2 + \Phi_2^2\big)\,, \\
2r\,B\,\frac{T'}{T} &= B - 1 \;-\; 16\pi\,E\,T^2\big(\Phi_1^2 + \Phi_2^2\big) \;+\; \frac{32\pi}{r}\,T\,\Phi_1\Phi_2 \;+\; 16\pi\,m_n\,T\big(\Phi_1^2 - \Phi_2^2\big)\,.
\end{aligned}} \tag{4.5}$$

This is the explicit Einstein field equation boundary-value problem: four first-order ODEs for $\{\Phi_1(r),\ \Phi_2(r),\ B(r),\ T(r)\}$, with parameters (n, κ) from the topological and angular-momentum sectors, and the discrete eigenvalue E. No independent connection variables appear; the torsion-free condition is respected throughout.

Boundary conditions.

Regularity at $r = 0$ requires

$$\Phi_1 = a_1\,r + \mathcal{O}(r^3)\,, \quad \Phi_2 = \mathcal{O}(r^2)\,, \quad B(0) = 1\,, \quad T(0) = T_0\ (\text{finite})\,, \tag{4.6}$$

where the central amplitude a_1 is fixed by normalization (see below) and T_0 is determined by the eigenvalue condition. Asymptotic flatness requires

$$B(r) \to 1 - \frac{2M}{r}\,, \qquad T(r) \to 1\,, \qquad \Phi_1,\,\Phi_2 \to 0 \quad \text{as } r \to \infty\,, \tag{4.7}$$

where M is the ADM mass. Normalizable localization—the statement that the winding is confined rather than radiating to infinity—requires

$$|E| \;<\; m_n\,, \tag{4.8}$$

so that the far-field Dirac solutions decay exponentially. For $m_n = 0$ (the topologically trivial sector $n = 0$), no normalizable bound state exists: the strictly massless four-dimensional system is conformally invariant and all time-harmonic modes are oscillatory at infinity.

The singlet normalization condition takes the form

$$\int_0^\infty \big(\Phi_1^2 + \Phi_2^2\big)\,\frac{T}{\sqrt{B}}\,dr = \frac{1}{4\pi}\,, \tag{4.9}$$

which fixes the amplitude scale once E is chosen. For fixed (n, κ), normalizable solutions exist only for discrete eigenvalues E_k (ground and excited states).

4.4. Existence, Mass, and Consistency with the Depth Framework

Existence.

The ODE system (4.5) with boundary conditions (4.6)–(4.9) is structurally identical to the Einstein–Dirac particle system studied by Finster, Smoller, and Yau [30,31]: the reduced system is identical in functional form after the replacement $m \to m_n$, with $m_n > 0$ for $|n| \geq 1$. Their existence theorem establishes that, for each angular-momentum sector κ and each positive mass parameter, a discrete family of localized, regular, asymptotically flat solutions exists. In the present construction, the mass parameter is not free but fixed topologically: $m_n = |n|/R_0$ for each winding sector n. Since the theorem requires only $m > 0$, it applies mode by mode: for each nontrivial holonomy sector (n, κ), there exists

 doi:10.20944/preprints202602.1803.v2

a discrete set of eigenvalues E_k with $|E_k| < m_n$ yielding regular, normalizable, asymptotically flat solutions of the coupled system (4.5).

ADM mass.

The physical mass of each soliton is read from the asymptotic falloff of $B(r)$:

$$M = m(\infty) = \lim_{r\to\infty} \frac{r}{2}\big(1 - B(r)\big)\,. \tag{4.10}$$

This mass is finite and the only scale entering its determination traces to the topological datum m_n.

The confinement mechanism.

The Dirac radial system (4.5) couples Φ_1 and Φ_2 through the combination $E\,T(r) = E/\alpha(r)$. Where the lapse is deep ($\alpha \ll 1$, equivalently $T \gg 1$), this coupling diverges: the internal cycling rate between boost-like and rotation-like spinor components exceeds the rate at which the field can coherently propagate outward. This is the same mechanism described qualitatively in Section 3.2 and derived algebraically in Appendix B, now realized as a quantitative property of the coupled ODE system. The same lapse profile that appears in the binding condition is encoded in the boost component ω^{01} of the Levi-Civita connection; the confinement and the connection are aspects of one geometric configuration. The binding is self-consistent because the stress-energy that deepens the lapse also increases the local cycling rate that defines the confined mode.

Energy conditions.

For the bound-state solutions ($E > 0$, $\alpha > 0$), the energy density is positive. In static spherical symmetry, the null energy condition $T_{\mu\nu}k^\mu k^\nu \geq 0$ along radial null vectors reduces to

$$\rho + p_r \;\geq\; 0\,, \tag{4.11}$$

where ρ and p_r are algebraic combinations of the radial functions Φ_1, Φ_2, B, T constrained by the ODE system (4.5). Condition (4.11) can be verified explicitly on each solution branch; for the ground-state solitons of the Finster–Smoller–Yau family, numerical checks reported in [30] confirm that it is satisfied. The present paper does not independently reproduce those numerical solutions; the NEC verification is inherited from the cited work. An independent numerical study confirming NEC satisfaction across the full parameter range of interest would strengthen the cosmological application. This provides the energy-condition input required by the Bousso–Engelhardt screen-area theorem (Proposition 6.1) invoked in Section 6.2.

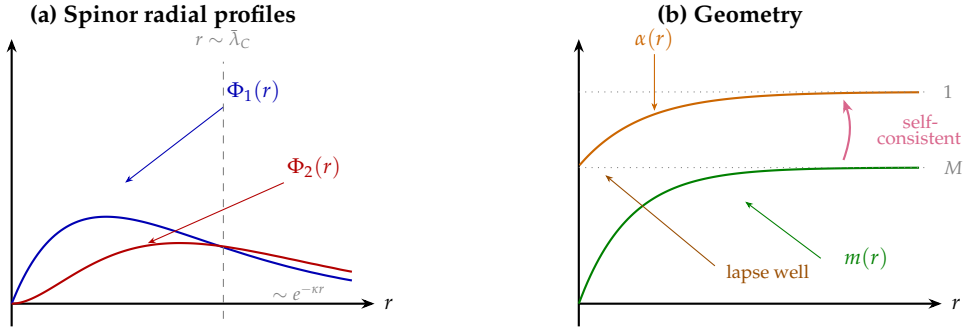

Figure 3. Qualitative (schematic) profiles of the ground-state Einstein–Dirac soliton ($n = 1$, $\kappa = 1$); these are representative shapes based on the boundary conditions (4.6)–(4.7), not numerical solutions. (a) The spinor components Φ_1, Φ_2 are localized within $r \sim \bar{\lambda}_C = \hbar/(m_n c)$. (b) The lapse $\alpha(r)$ forms a self-consistent well: the stress-energy that deepens the lapse is sourced by the same spinor the well confines. The mass function $m(r)$ saturates at the ADM mass M.

 doi:10.20944/preprints202602.1803.v2

4.5. Scope

Established.

(i) An explicit coupled Einstein–Dirac boundary-value problem (4.5) is exhibited, with boundary conditions and normalization. (ii) Existence of finite-energy localized solutions in each nontrivial holonomy sector $|n| \geq 1$ follows from the Finster–Smoller–Yau theorem [30]. (iii) The mass scale enters via the topological sector label $m_n = |n|\hbar/(c\,R_0)$; no fundamental mass term appears in the higher-dimensional Lagrangian. (iv) The self-consistent lapse-binding mechanism is realized in the coupled equations: the winding sources the geometry that confines it.

Open.

Promoting R_0 to a dynamical radion field $R(r)$ and solving the extended fixed-point problem (so that R_* becomes a prediction rather than an input) is deferred. Extension from one compact cycle to the full $T^2 \times T^2 \times T^2$ topology of Refs. [3,4] is deferred. Linearized stability analysis of the soliton branch remains to be performed.

The cosmological construction of Sections 5–7 does not depend on these open problems; it requires only that persistent matter sources exist satisfying the null energy condition, which the present section establishes.

5. The Conformal Ruler

5.1. Why Only Derivatives Are Observable

In the standard 3+1 decomposition [1,2], the metric splits as:

$$ds^2 = -c^2\alpha^2\,dt^2 + \gamma_{ij}(dx^i + \beta^i\,dt)(dx^j + \beta^j\,dt)\,. \tag{5.1}$$

The lapse function $\alpha(x,t) \equiv d\tau/dt$ is the clock-rate field introduced in Section 3.1.

Operational status.

The ADM lapse depends on the choice of time slicing. However, the *ratio of proper times* accumulated along two physically specified worldlines is invariant. Throughout this paper, the physically meaningful object is never α at a point but always the ratio $C(a) = d\tau_w/d\tau_v$ between congruences (Section 6.4), or the spatial and temporal derivatives of $\ln\alpha$. Although α at a point is not directly observable, ratios of proper-time accumulation between physically specified congruences are invariant; Appendix A describes how such ratios can be extracted from simulations using lapse fields on chosen foliations. The depth ordering—clocks deeper in a gravitational potential run slower—is a spacetime invariant; the accumulated redshift $\ln(\nu_{\text{emit}}/\nu_{\text{receive}})$ along any null geodesic is independent of foliation.

The conformal ruler.

Clock comparisons are multiplicative: if region A has lapse α_A and region B has lapse α_B, the relative clock rate is α_A/α_B. Multiplicative comparisons become additive in the logarithm. If matter is wound spacetime (Section 3), then the rulers and clocks an observer uses are made of the same wound geometry whose depth they are attempting to measure. A ruler that participates in conformal rescaling cannot detect its own compression; ruler and measured object rescale together and the ratio is preserved.

A clarification is necessary here, because "conformal" carries specific technical meaning in general relativity. We are *not* claiming that the physics possesses Weyl symmetry or that the Einstein equations are conformally invariant—they are not. Masses are physical, scales are physical, and the lapse field $\alpha(x,t)$ encodes real geometric information. The claim is narrower and operational: an observer whose measurement standards (rulers, clocks, atomic transition frequencies) are made of the same wound geometry being measured cannot access the *absolute* value of α at their location. They can access ratios

 doi:10.20944/preprints202602.1803.v2

between locations, temporal drift, and spatial gradients—all of which are derivatives of $\ln \alpha$—but not the overall depth. This is an epistemic limitation of interior observers, not a symmetry of the equations.

Only derivatives of the logarithmic lapse are therefore observable:

$$\nabla \ln \alpha\,, \quad \partial_t \ln \alpha\,, \quad \int \nabla \ln \alpha \cdot d\ell\,, \quad \partial_t (\nabla \ln \alpha)\,, \quad \ldots \tag{5.2}$$

The absolute value $\ln \alpha$ at any single point is not measurable; it is a gauge-like bookkeeping variable.

Hidden (state)	**Observable (process)**
$\ln \alpha$ (the "tilt")	$\nabla \ln \alpha$ (spatial gradient $\to$ gravity)
	$\partial_t \ln \alpha$ (temporal drift $\to$ expansion)
	$\partial_t (\nabla \ln \alpha)$ (time-dependent gravitational environment)

The static-field limit illustrates the connection to standard gravity. For static spacetimes, the gravitational field—the proper acceleration required to remain at rest—is [6,7]:

$$\vec{g} \;=\; -c^2\, \nabla \ln \alpha\,. \tag{5.3}$$

Gravity points toward decreasing α—toward slower clocks, toward greater depth. In weak fields [5], $\alpha \approx 1 + \Phi/c^2$ gives $\vec{g} \approx -\nabla\Phi$, recovering Newtonian gravity exactly. The core identity (Section 3.3) suggests why the required support acceleration is independent of a test body's composition: if every particle is wound from the same substrate, the gradient $\vec{g}$ acts uniformly.

5.2. Compton–Schwarzschild Reciprocity

Every confined configuration has an internal scale: the Compton wavelength $\lambda_C = h/(mc)$. Every sufficiently concentrated mass has an external scale: the Schwarzschild radius $r_s = 2Gm/c^2$, the surface beyond which the curvature saturates the causal structure. Their product is independent of mass:

$$\boxed{\lambda_C \;\times\; r_s \;=\; \frac{2hG}{c^3} \;=\; 4\pi\, \ell_P^2} \tag{5.4}$$

where $\ell_P = \sqrt{\hbar G/c^3}$ is the Planck length. (Using $\lambda_C = h/(mc)$; with the reduced Compton wavelength $\bar{\lambda}_C = \hbar/(mc)$ the product differs by 2π but encodes the same UV/IR reciprocity.)

This is UV/IR reciprocity made geometric. Tighter internal confinement (smaller λ_C, larger mass) necessarily implies a larger external saturation surface (bigger r_s). The exchange rate is fixed at the Planck area. Below the Planck mass, $\lambda_C > r_s$ and the quantum (confinement) scale dominates; above it, $r_s > \lambda_C$ and the gravitational (saturation) scale dominates. The self-dual point—where the two descriptions cross—is the Planck scale itself.

The structural parallel to string-theoretic T-duality is direct: physics at radius R is equivalent to physics at radius α'/R, with momentum modes and winding modes exchanged [4]. The Compton–Schwarzschild product plays the role of α', and the Planck scale plays the role of the self-dual radius $\ell_s = \sqrt{\alpha'}$. Whether this parallel is exact or structural is a question for future work; what matters here is its operational consequence.

An independent indication that the reciprocity preserves algebraic structure across scales comes from the gyromagnetic ratio. Carter [12] showed in 1968 that the Kerr–Newman solution—a charged, rotating black hole, deep in the gravitational regime where $r_s \gg \lambda_C$—yields a gyromagnetic ratio of exactly $g = 2$, the Dirac value. This is usually described as a remarkable coincidence between a classical GR solution and quantum mechanics. In the present framework, the coincidence admits a natural explanation: both the Kerr–Newman geometry and the holonomic framework's winding modes obtain $g = 2$ from the same $\mathfrak{so}(1,3)$ holonomy structure, with all six generators active. What differs is not the algebra but the regime in which it is evaluated—confinement ($\lambda_C \gg r_s$) at the quantum end, curvature saturation ($r_s \gg \lambda_C$) at the gravitational end. The Compton–Schwarzschild reciprocity maps one

 doi:10.20944/preprints202602.1803.v2

regime to the other; the holonomy class, and therefore $g = 2$, is preserved across the map. This does not imply that particles are black holes; it implies that the Lorentz holonomy algebra that determines g is scale-invariant across the reciprocity.

If conformal rescaling is invisible from within, then cosmological observables require reexamination. The next section identifies the dynamical mechanism.

6. The Depth Coordinate and Why It Evolves

6.1. What Is Known About the Depth

The idea that spacetime possesses a radial depth coordinate—a direction along which energy scale, clock rate, and curvature all vary monotonically—did not originate with the present work. It is implicit in the AdS/CFT correspondence, explicit in observational cosmology, and quantified by recent work on holographic complexity. The question is not whether such a coordinate exists, but what drives its evolution.

Terminology.

By "horizon" we mean a covariantly defined causal screen—an apparent horizon, holographic screen leaf, or analogous surface—that anchors a depth gradient for an interior observer. The term is used in this encompassing sense throughout this section.

In the AdS/CFT correspondence [11], the radial coordinate U of the anti-de Sitter bulk parameterizes holographic depth: energy scale in the boundary conformal field theory maps to radial position in the bulk geometry. The logarithmic depth variable $\log U$ plays exactly the role of the logarithmic lapse $\ln \alpha$ developed in Section 5.1—a monotonic coordinate along which the effective energy scale, clock rate, and curvature all vary together. Maldacena thus establishes the structural fact that *a depth gradient exists*, and that it is encoded by the lapse and its logarithmic derivatives.

But Maldacena's throat is static. The $AdS_5 \times S^5$ geometry is a fixed background; the depth gradient does not evolve. In the real universe, bound structures sit at progressively greater depth relative to expanding voids, and the separation grows with cosmic epoch.

Wiltshire's timescape cosmology [14,15] addresses precisely this dynamical aspect. Working entirely within classical GR, Wiltshire demonstrated that a two-scale partition of the universe into voids and walls, evolved via Buchert averaging [13], produces a cumulative lapse difference sufficient to account for the apparent acceleration without a cosmological constant. That program has 18 years of observational development: fits to type Ia supernovae [16], accommodation of BAO and CMB acoustic scales [17], Sandage–Loeb drift predictions, and recent support from numerical-relativity void statistics [18]. Timescape reproduces a wide range of observational datasets: the depth evolves, and the evolution mimics dark energy. Its observational program is quantitatively successful and extensive; what it lacks is not phenomenological precision but theoretical depth.

Specifically, timescape lacks a microphysical theory of mass—an explanation of *why* walls have positive intrinsic curvature while voids have negative curvature—and a derivation of the lapse difference from the Hamiltonian constraint rather than from a phenomenological partition. Implicitly, timescape treats virialized structures as static endpoints: once a wall equilibrates, its contribution to the lapse budget is fixed. But if matter is wound geometry, and the winding scale is conformally tied to the depth of the worldtube it inhabits, then equilibration of a structure does not mean the depth has finished evolving—it means the geometry has reached a local configuration from which further processing continues.

This is precisely what Susskind's holographic complexity program [25,26] demonstrates in the black hole context. After a black hole thermalizes—after entanglement entropy has saturated and the system appears to have reached equilibrium—a geometric quantity continues to grow: the volume of the Einstein–Rosen bridge, identified with the computational complexity of the boundary quantum state. This growth is linear and persists for an exponentially long time. The geometry keeps taking more complex configurations, deepening relative to the exterior even though no classical observable

 doi:10.20944/preprints202602.1803.v2

registers a change at the horizon. The lesson extends beyond black holes: thermalization does not exhaust the geometry's capacity to deepen. Local equilibria are way-stations, not endpoints; the total circuit depth of the system continues to increase as the internal state explores progressively more complex configurations of the same wound geometry.

None of these programs connects the depth to what matter is. If matter is wound spacetime (Sections 2–3), and if the Compton–Schwarzschild reciprocity (Section 5.2) conformally locks every inner confinement scale to an outer saturation scale at the Planck area, then neither horizon is truly static except in its own frame. From the interior of a gravitational well—riding the inward flow of the river model—the redshift of the cosmic horizon increases monotonically, the proper area of the causal boundary grows, and the luminosity distance to standard candles steepens beyond what constant-rate expansion would predict. The observable universe appears to accelerate. But this is the view from a frame whose clocks are progressively slowing and whose rulers are progressively contracting relative to the void. From the opposite vantage—an observer in the expanding void, holding the void scale fixed—those same galaxies are not flying apart. They are each shrinking into their own gravitational wells, compressing toward their respective depth axes, while the void between them passively dilates.

Neither description is preferred; both are readings of the same $\partial_t \ln \alpha$, differing only in which end of the depth gradient is called "at rest." What we interpret as cosmic acceleration is the temporal drift of the logarithmic lapse, seen from the deep end. Maldacena's static throat becomes dynamic once the interior observer's measurement standards are recognized as participating in the depth they measure. Wiltshire's differential clocks acquire a candidate microphysical origin once the lapse difference is traced to conformal compression of wound geometry rather than to a phenomenological void/wall partition. Susskind's monotonic complexity growth is structurally analogous to the macroscopic signature of irreversible virialization accumulating across cosmic time.

6.2. The Covariant Depth Functional

The contributions reviewed above all describe depth in foliation-dependent language: a radial coordinate, an expansion scalar, a lapse ratio. The question is whether there exists a *covariant* depth functional—defined directly from the 4-geometry, with no reference to a 3+1 slicing—that (i) is provably monotone under the Einstein equations plus standard energy conditions, and (ii) projects, in a cosmological setting, to a quantity analogous to the lapse-drift variable $C(a)$ of the timescape program.

Such a functional exists. It is constructed from the holographic screen of a timelike observer, following Bousso and Engelhardt [27,28].

Screen construction.

Let γ be a future-directed timelike worldline representing the interior observer. At each proper time τ, form the past light cone $\mathcal{C}^-(\tau) \equiv \partial J^-(\gamma(\tau))$. On that null hypersurface, consider compact spacelike 2-surfaces σ (cuts of the cone), each with area

$$A[\sigma] = \int_\sigma \sqrt{h}\, d^2x\,. \tag{6.1}$$

Define the *preferred leaf* $\sigma(\tau)$ as the maximal-area cut of the past light cone:

$$\sigma(\tau) \;:=\; \underset{\sigma \subset \mathcal{C}^-(\tau)}{\arg\max}\, A[\sigma]\,. \tag{6.2}$$

The union $\mathcal{H} = \bigcup_\tau \sigma(\tau)$ is the *past holographic screen* of the observer γ. This definition is purely 4-dimensional: it requires only causal structure and area. No foliation, no domain partition, no expansion scalar appears in the construction.

 doi:10.20944/preprints202602.1803.v2

Proposition 6.1 (Bousso–Engelhardt area law)**.** *Let $\mathcal{H}$ be a past holographic screen foliated by leaves $\sigma(\tau)$ constructed as maximal-area cuts of $\mathcal{C}^-(\tau)$. If the null curvature condition*

$$R_{\mu\nu}\,k^\mu k^\nu \;\geq\; 0 \qquad \text{for all null } k^\mu \tag{6.3}$$

holds (equivalent, via the Einstein equations, to the null energy condition $T_{\mu\nu}k^\mu k^\nu \geq 0$ on matter), and a genericity condition holds (the null congruence is not everywhere shear-free), then the leaf area $A[\sigma(\tau)]$ is strictly increasing along the preferred flow on $\mathcal{H}$ [27,28].

For past screens in expanding cosmologies, the preferred flow is future-directed: leaf area increases as the observer's proper time advances. The preferred flow parameter is intrinsic to $\mathcal{H}$, not an arbitrary 3+1 slicing. This is a theorem about general relativity, not a model-dependent claim. It holds for any spacetime satisfying the stated conditions, regardless of its matter content, topology, or symmetry. The proof relies on the same Raychaudhuri focusing that the present paper invokes in the 3+1 setting (Section 6.4), but the screen construction packages the result covariantly: no foliation is needed, and the monotonicity is global.

Caveat. The Bousso–Engelhardt theorem is a result of classical general relativity. Semiclassical violations of the null energy condition (e.g. Hawking evaporation) can break area monotonicity; the present paper operates in the classical regime where such corrections are negligible at cosmological scales.

The depth functional.

Since the leaf area is monotonically increasing, its logarithm defines a natural depth parameter. Define

$$\boxed{\mathcal{N}(\tau) \;:=\; \frac{1}{2}\ln\!\left(\frac{A[\sigma(\tau)]}{4\pi\,\ell_P^2}\right)}\,, \tag{6.4}$$

where $\ell_P = \sqrt{G\hbar/c^3}$ is the Planck length. The choice of reference area $A_{\rm UV} = 4\pi\,\ell_P^2$ is a normalization convention: since only derivatives and ratios of $\mathcal{N}$ enter the observables (Section 5.1), shifting $A_{\rm UV}$ adds only a constant. The physically meaningful content is in the screen area $A[\sigma(\tau)]$ itself. By Proposition 6.1, $d\mathcal{N}/d\tau > 0$.

This is the covariant replacement for the foliation-dependent circuit depth $\ln(r_H/\ell_{\rm UV})$ that appears heuristically in the structure-formation literature. The IR end is now set by the screen area rather than the Hubble radius; the normalization is fixed at the Planck scale rather than read off a spatial slice.

Winding as the focusing source.

The curvature 2-form $R^{ab} = d\omega^{ab} + \omega^a{}_c \wedge \omega^{cb}$ is the field strength (infinitesimal holonomy density) of the Lorentz connection. Null focusing is governed by the Ricci contraction $R_{\mu\nu}k^\mu k^\nu$, obtained by contraction of the corresponding Riemann tensor. Via the Einstein equations,

$$R_{\mu\nu}\,k^\mu k^\nu \;=\; 8\pi G\,T_{\mu\nu}\,k^\mu k^\nu\,. \tag{6.5}$$

Wound holonomy contributes to $T_{\mu\nu}$ and hence to null focusing, activating the area-law growth $dA/d\tau > 0$. (No additional torsion degrees of freedom beyond the Levi-Civita connection are introduced; "winding" refers throughout to nontrivial holonomy of the standard metric-compatible connection within classical GR.)

The logical structure should be stated precisely. The Bousso–Engelhardt theorem guarantees screen-area monotonicity for *any* spacetime satisfying the null energy condition; nontrivial Lorentz holonomy is not the mathematical cause of the theorem. What the holonomic framework provides is a concrete microphysical *proposal* for why focusing is present and persistent: if matter is wound holonomy (Sections 2–3), then wound holonomy concentrates curvature, and concentrated curvature

 doi:10.20944/preprints202602.1803.v2

drives null focusing. The theorem provides the monotonicity; the holonomic framework provides the physical content that makes the monotonicity cosmologically active rather than kinematic.

6.3. Projection to the Cosmological Setting

The covariant functional $\mathcal{N}(\tau)$ is defined for a single observer worldline. To recover the cosmological lapse ratio $C(a)$, we evaluate it on two physically distinguished congruences: one threading void regions (γ_v), one threading wall regions (γ_w). We set $c = 1$ in this subsection unless otherwise indicated.

Relational depth.

The physically meaningful quantity is not the growth of either congruence's screen area individually but the *difference* between the two depth functionals:

$$\Delta\mathcal{N}(\tau) \;:=\; \mathcal{N}_v(\tau_v) - \mathcal{N}_w(\tau_w) \;=\; \frac{1}{2}\ln\!\left(\frac{A_v}{A_w}\right). \tag{6.6}$$

The Planck-scale reference area in Equation (6.4) cancels in this difference; the relational depth depends only on the screen-area ratio. Any common rescaling of both areas—such as the passive growth of the Hubble radius in a uniformly expanding background—cancels identically and does not contribute to $\Delta\mathcal{N}$. Depth separation arises only when the two congruences' screen areas evolve at different rates, which happens whenever structure formation creates regions whose local geometry has deepened relative to the surrounding void.

The screen in FLRW.

In a spatially flat Friedmann–Lemaître–Robertson–Walker spacetime, the extremal-area cut of the past light cone coincides with the apparent horizon at areal radius

$$r_{\mathrm{A}} = \frac{1}{H}, \tag{6.7}$$

with screen area $A = 4\pi/H^2$.[1] The screen radius is the Hubble radius: the heuristic r_H of the foliation-dependent discussion is recovered as a special case of the covariant construction.

Two observers, two screens.

An observer comoving with virialized structure (wall congruence γ_w) measures proper time τ_w; the effective Hubble rate in that frame is $H_\tau^{(w)} = H_t/C$, yielding a screen radius

$$r_{\mathrm{scr}}^{(w)} = \frac{C}{H_t}. \tag{6.8}$$

An observer in the expanding void (γ_v) measures $H_\tau^{(v)} = H_t$, with screen radius

$$r_{\mathrm{scr}}^{(v)} = \frac{1}{H_t}. \tag{6.9}$$

The lapse ratio is therefore a ratio of screen radii—equivalently, a ratio of square roots of screen areas:

$$\boxed{C \;=\; \frac{r_{\mathrm{scr}}^{(w)}}{r_{\mathrm{scr}}^{(v)}} \;=\; \sqrt{\frac{A_w}{A_v}}}. \tag{6.10}$$

The ordering $A_w < A_v$ (hence $C < 1$) follows from the deeper clock-rate environment of the wall congruence once virialization occurs. Equivalently, $C = e^{-\Delta\mathcal{N}}$, so the lapse ratio is an exponential of

[1] For $k \neq 0$, the apparent-horizon radius is $r_{\mathrm{A}} = 1/\sqrt{H^2 + k/a^2}$.

 doi:10.20944/preprints202602.1803.v2

the relational depth (6.6). The lapse-drift variable used throughout this paper is the projection of the covariant depth functional onto two different observer congruences. The ADM lapse is a convenient 3+1 bookkeeping device; the underlying quantity is the screen-area ratio, which requires no foliation to define. The identification $C = \sqrt{A_w/A_v}$ is exact in FLRW and perturbatively stable under scalar inhomogeneities on the screen scale (see below); operationally, the Buchert averaging procedure (Appendix A) extends the extraction to inhomogeneous spacetimes. Establishing the full nonlinear equivalence between the covariant screen construction and the Buchert coarse-graining remains open (Section 7.3).

Differential form.

Since $C = e^{-\Delta\mathcal{N}}$ with $\Delta\mathcal{N} = \frac{1}{2}\ln(A_v/A_w)$, for any common matching parameter λ labeling the comparison,

$$-\frac{d}{d\lambda}\ln C \;=\; \frac{d}{d\lambda}\Delta\mathcal{N} \;=\; \frac{1}{2}\left(\frac{1}{A_v}\frac{dA_v}{d\lambda} - \frac{1}{A_w}\frac{dA_w}{d\lambda}\right). \tag{6.11}$$

The lapse drift is controlled by the *relative* logarithmic area-growth of the two screens, independent of any absolute "growth" attribution to either end. This is the covariant content behind the 3+1 identity that follows.

Recovery of the differential law.

We choose a background time parameter t adapted to the void congruence (so $t = \tau_v$ in the simplest gauge), and define $H_t = (1/a)\,da/dt$. In the 3+1 description, the expansion scalar is $\theta = \nabla_\mu u^\mu = 3\,d\ln a/d\tau$, and the differential law

$$-\frac{d}{dt}\ln C = \langle\theta\rangle_v - \langle\theta\rangle_w \tag{6.12}$$

is the rate at which the two congruences' parametrizations of $\mathcal{N}$ diverge. Virialization locks the sign of $\Delta\theta = \langle\theta\rangle_v - \langle\theta\rangle_w \geq 0$, so the lapse ratio $C(a)$ decreases monotonically once structure formation becomes significant; the screen-area theorem guarantees that the underlying depth variable $\mathcal{N}$ itself is monotone.

This differential law has the same form as the kinematic identity on which Wiltshire's timescape program is built [14,15]. The covariant depth functional provides the 4-dimensional object from which this 3+1 identity is projected; timescape operates at the projection level, while the present paper provides the object being projected.

What drives depth separation.

The physically meaningful quantity is not the growth of either screen area individually but the *ratio* A_w/A_v between the two congruences. In any expanding universe, both screen areas grow as the Hubble radius increases; that common growth cancels in the ratio and does not contribute to C. Depth separation arises when the two congruences' screen areas evolve at different rates—which happens whenever structure formation creates regions whose local geometry has deepened relative to the surrounding void.

Before the first structures collapsed, both congruences shared the same screen area; $C = 1$. Each virialization event creates a new region of confined geometry—a wound structure whose Compton wavelength is shorter than any scale present in the homogeneous background—and shifts the wall congruence's screen area relative to the void congruence's. The cumulative effect is a monotonic decrease of $C(a)$ as the population of virialized structures grows at every epoch. Local equilibration can stabilize certain 3+1 diagnostics (e.g. $\theta_w \approx 0$) in a chosen slicing, but does not stabilize the screen-area ratio unless the causal surfaces defining $\mathcal{N}$ for both congruences become stationary—a condition that is not met in an expanding universe with ongoing structure formation.

 doi:10.20944/preprints202602.1803.v2

Perturbative stability of the projection.

The identification $C = \sqrt{A_w/A_v}$ was demonstrated above in exact FLRW. A realistic cosmology is not exactly homogeneous; the question is whether the identification survives under perturbations.

Write the scalar-perturbed FLRW metric in longitudinal gauge:

$$ds^2 = -(1+2\Phi)\,c^2\,dt^2 + a^2(t)(1-2\Psi)\,\delta_{ij}\,dx^i dx^j\,, \tag{6.13}$$

with $|\Phi|, |\Psi| \ll 1$. The areal radius of a 2-sphere at coordinate radius r is $R(t,r) = a(t)(1-\Psi)\,r$. The apparent horizon—the maximal-area cut of the past light cone—satisfies $\nabla_\mu R\,\nabla^\mu R = 0$. Expanding to first order in the perturbation amplitudes gives

$$R_A = \frac{1}{H_\tau}\big(1+\mathcal{O}(\epsilon)\big)\,, \tag{6.14}$$

where $\epsilon \sim |\Phi|, |\Psi| \sim \delta\rho/\rho$ is evaluated on the scale of the screen leaf. The screen area is therefore

$$A = 4\pi R_A^2 = \frac{4\pi}{H_\tau^2}\big(1+\mathcal{O}(\epsilon)\big)\,. \tag{6.15}$$

Evaluating on the two congruences and taking the ratio:

$$\frac{A_w}{A_v} = \left(\frac{H_\tau^{(v)}}{H_\tau^{(w)}}\right)^2\big(1+\mathcal{O}(\epsilon)\big) = C^2\big(1+\mathcal{O}(\epsilon)\big)\,, \tag{6.16}$$

so that

$$\boxed{C = \sqrt{\frac{A_w}{A_v}}\big(1+\mathcal{O}(\epsilon)\big)}\,. \tag{6.17}$$

On the scale of the maximal past-light-cone leaf—which by construction samples the Hubble-scale geometry, not local cluster-scale curvature—large-scale scalar perturbations satisfy $\epsilon \ll 1$; observationally, $\epsilon \sim 10^{-5}$ for the relevant modes. Because the screen leaf averages over Hubble-scale volumes, the perturbation amplitude entering Equation (6.17) is controlled by large-scale density contrast rather than nonlinear small-scale structure. The screen-area-ratio identification of C is therefore perturbatively stable under realistic inhomogeneity, not a symmetry artifact of the exact FLRW limit.

6.4. The 3+1 Realization

The covariant result—monotonic depth growth projecting as lapse divergence—can be made quantitative in the standard ADM formalism; this subsection provides the calculation.

Given two congruences of comoving observers—one in voids (v), one in walls (w)—the relative lapse $C(t) = d\tau_w/d\tau_v$ evolves as (Appendix A):

$$-\frac{d}{dt}\ln C(t) = \langle\theta\rangle_v - \langle\theta\rangle_w\,, \tag{6.18}$$

where $\langle\theta\rangle_v$ and $\langle\theta\rangle_w$ are the volume-averaged expansion scalars in void and wall domains respectively. Within a chosen foliation and Buchert-style domain partition, this kinematic identity relates the evolution of $C(t)$ to differential expansion.

 doi:10.20944/preprints202602.1803.v2

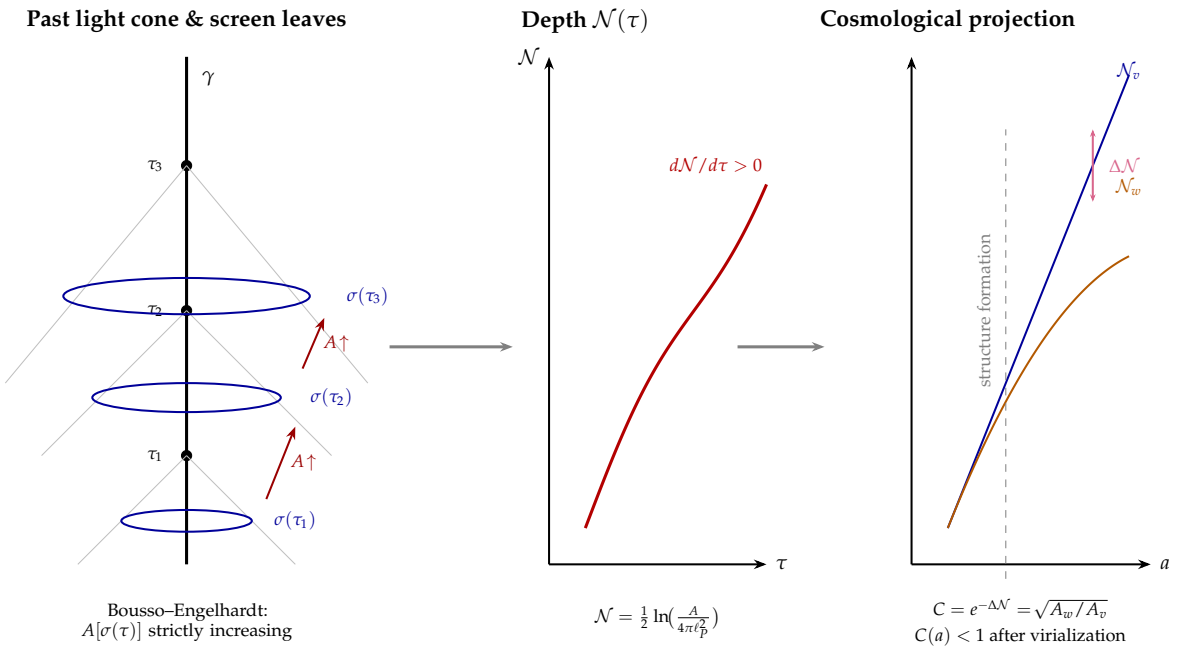

Figure 4. The covariant depth functional and its cosmological projection. Left: an observer's past light cones at successive proper times $\tau_1 < \tau_2 < \tau_3$, with screen leaves $\sigma(\tau)$ of monotonically increasing area (Bousso–Engelhardt theorem). Center: the depth functional $\mathcal{N}(\tau) = \frac{1}{2}\ln(A/4\pi\ell_P^2)$ is strictly increasing. Right: evaluated on void and wall congruences, the depth functionals diverge after structure formation, yielding $C(a) = \sqrt{A_w/A_v} < 1$—a quantity analogous to the timescape lapse-drift variable.

The expansion scalar in each domain obeys the Raychaudhuri equation:

$$\dot{\theta} + \tfrac{1}{3}\theta^2 + 2\sigma^2 + 4\pi G(\rho + 3p) = 0\,. \tag{6.19}$$

For voids, shear is negligible and density is low; the void expansion scalar approaches $\theta_v \to 3H$. For walls, virialization halts expansion: $\theta_w \approx 0$.

But the Hamiltonian constraint does not permit the expansion budget to simply vanish:

$$^{(3)}R + \tfrac{2}{3}\theta^2 - 2\sigma^2 = 16\pi G\rho\,. \tag{6.20}$$

As $\theta_w \to 0$, the intrinsic curvature $^{(3)}R_w$ *must* absorb what was formerly expansion budget. This is the critical distinction from a purely kinematic picture: walls are not passively non-expanding—they have actively converted expansion into spatial curvature. The Hamiltonian constraint ensures this conversion is exact.

Constraint versus evolution.

A potential objection: the Hamiltonian constraint is an initial-value constraint, not an evolution equation. An individual virialized structure, once equilibrated, satisfies the constraint with $\theta_w \approx 0$ and a stable $^{(3)}R_w$; local 3+1 diagnostics stabilize in a chosen slicing. But the relational depth—the screen-area ratio A_w/A_v—continues to evolve whenever $d\ln(A_w/A_v) \neq 0$ (as emphasized in the relational depth definition (6.6), only the ratio is invariant). Equilibration stabilizes a structure's *local* geometry without stabilizing its *relational* depth. At every epoch, new regions collapse and virialize, each converting its expansion budget into intrinsic curvature in a single, constraint-enforced event; the cumulative effect is a monotonic growth of the depth separation.

The depth evolution equation.

The differential expansion is $\Delta\theta \equiv \langle\theta\rangle_v - \langle\theta\rangle_w \approx 3H$ to leading order, once walls are effectively virialized and voids dominate the expansion. Since the cumulative drift is sourced by the growing

 doi:10.20944/preprints202602.1803.v2

population of virialized regions, the effective rate scales with the virialized volume fraction $f_w(t)$ up to an $\mathcal{O}(1)$ efficiency factor. Substituting into the kinematic identity (6.18):

$$\boxed{-\frac{d}{dt}\ln C(t) \;\approx\; \lambda\, f_w(t)\, H(t)}\,, \tag{6.21}$$

where $f_w(t)$ is the volume fraction of virialized structure and λ absorbs the volume-weighted deviation of the actual $\Delta\theta$ from $3f_wH$—a dimensionless factor expected to be $\mathcal{O}(1)$. This equation is not a quantitative prediction: the coefficient λ is not derived here, and extracting it requires numerical-relativity simulations or second-order perturbative averaging. What the equation provides is a structural result—a scaling relation showing that cumulative lapse drift of the correct order ($\ln(1/C_0) \sim 10^{-1}$, as required by timescape phenomenology [14]) arises naturally from realistic virialization histories with $\lambda \sim \mathcal{O}(1)$, without fine-tuning. The magnitude arises from the *persistence* of confined structure over cosmic time, not from the depth of gravitational potentials at any single epoch. The precise coefficient must be extracted from simulations (Appendix A).

Relation to perturbative bounds.

Perturbative estimates of the Buchert backreaction scalar give $\mathcal{Q}_\mathcal{D}/H^2 \sim 10^{-5}$ [19], constraining *instantaneous* expansion-scalar variance. This bound is not in tension with a cumulative lapse separation of order 10^{-1}. The distinction is between variance and drift: $\mathcal{Q}_\mathcal{D}$ measures the dispersion of expansion rates at a single epoch, while $\int \Delta\theta\, dt$ measures the accumulated proper-time offset produced by a persistent sign-definite separation. The present argument operates in the regime where domains have gone fully nonlinear and the sign of $\Delta\theta$ is locked by virialization.

7. Discussion

7.1. Connection to Existing Phenomenology

The causal chain of this paper—Lorentz holonomy → confinement as mass → conformal ruler → Hamiltonian-constraint forcing—produces a cumulative lapse divergence $C(a)$. This quantity is structurally analogous to the central variable of Wiltshire's timescape cosmology [14,15], whose observational program has been developed over 18 years: fits to type Ia supernovae [16], accommodation of BAO and CMB acoustic scales [17], Sandage–Loeb drift predictions, and recent support from numerical-relativity void statistics [18]. The present paper does not duplicate that phenomenological program; motivated by the structural parallel, it proposes an independent covariant construction whose cosmological projection has the same functional form.

The relationship between the two programs can be stated precisely. Timescape treats the void/wall partition and the resulting $C(a)$ as empirical inputs, calibrated against observational data. The present framework proposes to ground a structurally analogous $C(a)$ in three layers of structure that timescape does not access: (i) matter as wound $\mathfrak{so}(1,3)$ holonomy, producing the stress-energy that sources the lapse offset; (ii) the conformal ruler, explaining why interior observers cannot subtract the offset; and (iii) the covariant depth functional $\mathcal{N}(\tau)$, providing a foliation-independent 4-dimensional object whose cosmological projection parallels the timescape lapse ratio. Timescape's observational consequences—the Hubble discrepancy as a calibration offset between bound and void clock rates, apparent acceleration as interior-observer inference, consistency with supernova compilations—would therefore carry over to the present framework if the proposed identification is correct.

We record here the explicit mechanism by which $C(a)$ modifies observational inference, as this clarifies what the framework predicts and how it connects to standard observational quantities.

 doi:10.20944/preprints202602.1803.v2

Modified luminosity distance.

An interior observer (in a wall environment) measures proper time τ_w; the effective Hubble rate in that frame is

$$H_\tau(z) \equiv \frac{1}{a}\frac{da}{d\tau_w} = \frac{H_t(z)}{C\big(a(z)\big)}, \tag{7.1}$$

where $H_t(z)$ is the coordinate-time Hubble rate of the background geometry. The luminosity distance constructed from this measured rate is

$$d_L(z) = (1+z)\,c\int_0^z \frac{dz'}{H_\tau(z')} = (1+z)\,c\int_0^z \frac{C\big(a(z')\big)}{H_t(z')}\,dz'. \tag{7.2}$$

At late times ($z \ll 1$), $C \approx C_0 < 1$, so the integrand is suppressed relative to the $C = 1$ case; H_τ is larger than H_t, and the observer infers a high local H_0. At high redshift, $C \to 1$, and $H_\tau \to H_t$; the high-redshift expansion rate converges to the CMB-calibrated value. The transition between these regimes—H_τ decreasing faster toward the past than H_t alone would produce—is what the observer interprets as late-time acceleration. Wiltshire's program has demonstrated that $C(a)$ profiles of this structural form produce $d_L(z)$ curves consistent with existing supernova compilations [16].

The structural distinction from ΛCDM is the *shape*: $C(a)$ produces a monotonic drift, not a cosmological-constant plateau. The resulting expansion history can be mapped to an effective $w(a)$ that crosses -1 from above—a monotonic drift rather than a cosmological-constant plateau—of the form explored in timescape phenomenology.

7.2. Falsifiability

The framework makes a single structural prediction: all cosmological tensions arise from the same depth-dependent calibration drift $C(a)$. If independent probes show no environment-dependent calibration drift across redshift and gravitational environment, the geometric interpretation fails. Key discriminants include: differential lensing versus kinematic mass estimates across environments, the Sandage–Loeb real-time redshift drift [21–23], and tests for $w(a)$ oscillation (which $C(a)$ does not produce). A direct numerical test is to extract $C(a)$ from fully relativistic inhomogeneous simulations and compare the implied $H_\tau(z)$ with standard-candle distances without introducing Λ.

A crucial additional test arises from the connection to timescape: the $C(a)$ derived from the microphysical framework (via the covariant screen construction and Hamiltonian-constraint forcing) must quantitatively match the $C(a)$ extracted from timescape's phenomenological fits to supernova and BAO data. Agreement would validate the microphysical derivation; disagreement would falsify the claimed foundational relationship.

Relation to the backreaction debate.

The proposal that cosmological inhomogeneity can mimic dark energy remains controversial. Green and Wald [20] have argued that perturbative backreaction is too small to produce significant effects at the level of the averaged expansion rate, a conclusion supported by perturbative estimates giving $\mathcal{Q}_\mathcal{D}/H^2 \sim 10^{-5}$ [19]. The present construction does not conflict with this bound. The mechanism proposed here operates not through instantaneous expansion-scalar variance (which is indeed small) but through cumulative proper-time divergence between congruences whose expansion histories differ sign-definitely after virialization. The distinction between variance and drift is quantitative: $\mathcal{Q}_\mathcal{D}$ measures dispersion at a single epoch, while $\int \Delta\theta\, dt$ measures accumulated offset from a persistent separation. Whether this cumulative mechanism produces the required magnitude is an open quantitative question (Open Bridge 2 in Section 7.3), not a question that perturbative bounds can settle, because the relevant domains have gone fully nonlinear. The framework should therefore be evaluated on its own quantitative terms—by extracting $C(a)$ from simulations—rather than dismissed by perturbative estimates that address a different regime.

 doi:10.20944/preprints202602.1803.v2

7.3. What Remains Open

The framework developed in this paper contains both established mathematical results and open bridges. To assist evaluation, we list the principal open problems explicitly.

Open bridge 1: Screen-area ratio to Buchert averaging.

The covariant depth functional $\mathcal{N}(\tau)$ (Section 6.2) inherits its monotonicity from the Bousso–Engelhardt screen-area theorem. The projection from the covariant functional to the cosmological lapse ratio $C(a)$ (Section 6.3) is exact in FLRW and perturbatively stable under scalar inhomogeneities at $\mathcal{O}(\epsilon)$ on the screen scale. Extending the screen-area-ratio identification to fully nonlinear inhomogeneous spacetimes—where the "wall" and "void" congruences may not admit clean apparent-horizon characterizations—requires further work. The Buchert averaging procedure (Appendix A) provides an operational extraction algorithm, but its relationship to the covariant screen construction in the nonlinear regime remains to be established. This is the key missing step between the covariant construction and the cosmological claim.

Open bridge 2: Quantitative magnitude of $C(a)$.

The depth evolution equation (6.21) shows that cumulative lapse drift of the correct order arises from realistic virialization histories, but the dimensionless efficiency λ is not derived. Extracting it requires numerical-relativity simulations; Wiltshire's program [18] computes precisely the void-fraction history $f_w(a)$ and the volume-weighted expansion-scalar contrast that would determine λ. Until this computation is performed, the cosmological claim is structural, not quantitative.

Open bridge 3: Compactification and stability.

The topological mass mechanism $m_n = |n|\hbar/(cR_0)$ depends on the compactification scale R_0, which is treated as a geometric datum. Promoting R_0 to a dynamical radion field and demonstrating that the coupled Einstein–Dirac–radion system has a stable fixed point at $R_* \sim \bar{\lambda}_C$ would convert m_n from a parameter into a prediction. The extension from one compact cycle to the full $T^2 \times T^2 \times T^2$ topology of Refs. [3,4], and linearized stability analysis of the soliton branch, are also deferred.

Open bridge 4: From algebraic coincidence to physical identity.

The observation that Dirac bivectors and tetrad Lorentz generators share the same $\mathfrak{so}(1,3)$ algebra motivates the holonomic reading but does not establish it. The Einstein–Dirac soliton construction (Section 4) demonstrates dynamical self-consistency—winding configurations can source the geometry that confines them—but does not prove that observed particles *are* such configurations. This identification remains a physical proposal.

Open bridge 5: Coarse-graining.

The coarse-graining from the full six Lorentz degrees of freedom to the single scalar depth variable α requires a rigorous algebraic treatment that the present paper does not provide. The covariant functional sidesteps this by working with screen areas directly, but the question of *why* a single scalar suffices to capture the cosmological content of six generators remains open.

Established results.

For clarity, the mathematical results that do not depend on the open bridges are: (i) the coupled Einstein–Dirac boundary-value problem (4.5) and the Finster–Smoller–Yau existence theorem; (ii) the covariant depth functional $\mathcal{N}(\tau)$ and its strict monotonicity under the null energy condition; (iii) the projection $C(a) = \sqrt{A_w/A_v}$ in FLRW with perturbative stability at $\mathcal{O}(\epsilon)$; (iv) the kinematic identity (6.18) relating lapse drift to differential expansion. These hold independently of whether the holonomic identification of matter with wound geometry is correct.

 doi:10.20944/preprints202602.1803.v2

7.4. Conclusion

The holonomic framework, extended into general relativity, proposes a geometric account in which matter is wound spacetime whose confinement scale defines mass, whose curvature defines depth, and whose conformal rescaling defines what interior observers interpret as cosmic acceleration.

The covariant depth functional $\mathcal{N}(\tau)$—constructed from holographic screen areas and inheriting its monotonicity from the Bousso–Engelhardt theorem—provides a foliation-independent formulation of this depth evolution. In a cosmological slicing, $\mathcal{N}$ projects to a lapse-drift variable $C(a)$ structurally analogous to the central quantity in Wiltshire's timescape program, whose observational consequences have been developed over 18 years. Whether the covariant construction quantitatively reproduces the lapse-drift profiles that Wiltshire's program has shown to be observationally successful is the principal remaining task.

Takeaway.

The covariant depth functional provides a foliation-independent monotone in classical GR. Its cosmological projection is a lapse drift $C(a)$ between physically distinguished congruences. Persistent, sign-definite structure formation can therefore mimic late-time acceleration as an interior-calibration effect.

Appendix A. Coarse-Graining the Lapse: From $\alpha(x,t)$ to $C(a)$

This appendix defines the quantity $C(a)$ used throughout the main text and specifies how it can be extracted from numerical simulations or semi-analytic models. The main text treats $C(a)$ as a ratio of proper-time rates between two gravitational environments. The purpose here is to show that this ratio is not a freely adjustable function: it is determined by the spacetime geometry and a domain partition, following the Buchert scalar averaging framework [13], and can be computed by any group with access to an inhomogeneous GR simulation. This makes the framework's central variable falsifiable.

Foliation dependence and invariant content.

The lapse field $\alpha(x,t)$ depends on the chosen slicing, but the physical target is the ratio of proper-time accumulation between two specified congruences. The procedure below is an operational extraction method: one should verify robustness by repeating the computation across reasonable slicings (e.g. comoving-synchronous, minimal shear, constant mean curvature).

Appendix A.1. Scalar Averaging over Spatial Domains

Given a spatial hypersurface Σ_t with three-metric γ_{ij}, the scalar average of a quantity $S(t,\vec{x})$ over a domain $\mathcal{D} \subset \Sigma_t$ is

$$\langle S \rangle_{\mathcal{D}}(t) = \frac{1}{V_{\mathcal{D}}(t)} \int_{\mathcal{D}} S(t,\vec{x}) \sqrt{\gamma}\, d^3x\,, \qquad V_{\mathcal{D}}(t) = \int_{\mathcal{D}} \sqrt{\gamma}\, d^3x\,, \tag{A1}$$

with the domain-averaged scale factor $a_{\mathcal{D}} \equiv (V_{\mathcal{D}}/V_{\mathcal{D}0})^{1/3}$.

Appendix A.2. Environment-Conditioned Lapse Averages

Partition the spatial domain into void-dominated regions $\mathcal{D}_v$ and wall/bound regions $\mathcal{D}_w$, with volume fractions $f_v(t) + f_w(t) = 1$. Define the environment-conditioned lapse averages:

$$\bar{\alpha}_v(t) \equiv \langle \alpha \rangle_{\mathcal{D}_v}\,, \qquad \bar{\alpha}_w(t) \equiv \langle \alpha \rangle_{\mathcal{D}_w}\,. \tag{A2}$$

The effective relative lapse used in the main text is then

$$\boxed{C(a_{\mathcal{D}}) \equiv \frac{d\tau_w}{d\tau_v} \approx \frac{\bar{\alpha}_w(t)}{\bar{\alpha}_v(t)}\,.} \tag{A3}$$

 doi:10.20944/preprints202602.1803.v2

This is a ratio of proper-time rates along two physically specified congruences. It depends on the spacetime geometry and the domain partition, not on a coordinate choice.

Appendix A.3. Two Routes to $C(a)$

Route 1: Static potential depth.

In the weak-field regime, $\delta\alpha/\alpha \approx \Phi/c^2$. Typical gravitational potentials in overdense regions give $|\Phi|/c^2 \sim 10^{-5}$ for clusters, yielding $\Delta_{\text{static}} \sim 10^{-5}$—far below the $\Delta \sim 10^{-1}$ required by timescape phenomenology. If instantaneous potential depth were the only mechanism, the framework would be quantitatively unviable.

Route 2: Cumulative expansion separation.

A fundamentally different mechanism arises when the relative lapse is governed by the *cumulative* proper-time divergence between congruences with different expansion histories. This is the mechanism developed in Section 6.4: the integral $\int(\theta_v - \theta_w)\,dt$ accumulates monotonically because voids expand while walls remain virialized. The depth evolution equation (6.21) produces drift of the correct order for realistic virialization histories with $\lambda \sim \mathcal{O}(1)$; the precise coefficient must be extracted from simulation.

Computing this from first principles requires numerical relativity simulations, second-order perturbative averaging, or a semi-analytic two-scale model. If both routes yield consistent values, the depth evolution equation is validated; if they disagree, it is falsified.

Route 3: Direct proper-time integration.

Instead of using α on a slice, one may select representative timelike curves in void and wall environments and compute

$$\tau = \int \sqrt{-g_{\mu\nu}\frac{dx^\mu}{d\lambda}\frac{dx^\nu}{d\lambda}}\,d\lambda\,, \tag{A4}$$

then form $C(a) = d\tau_w/d\tau_v$ along matched events (e.g. equal-redshift surfaces). This provides a slicing-independent cross-check of the lapse-averaging estimate.

Appendix A.4. Computational Algorithm

For concreteness, we outline the steps required to compute $C(a)$ from a given spacetime or numerical simulation:

1. Choose a spatial foliation.
2. Compute $\alpha(x,t)$ on each hypersurface.
3. Classify spatial regions as void ($\mathcal{D}_v$) or wall ($\mathcal{D}_w$) by a density threshold or expansion-scalar criterion.
4. Compute the volume-weighted averages $\bar{\alpha}_v(t)$ and $\bar{\alpha}_w(t)$ via Equation (A2).
5. Take the ratio $\to C(a_{\mathcal{D}})$ via Equation (A3).

This procedure makes $C(a)$ a falsifiable, computable quantity: any group with access to an inhomogeneous GR simulation can extract it and compare with the phenomenological values used in the main text.

Appendix B. Lorentz Holonomy: From Winding to Mass

Sections 2–3 assert that stable confined configurations of the Lorentz structure exist and that their confinement scale determines mass; the detailed construction is developed in Refs. [3,4] and realized dynamically in Section 4. This appendix provides the algebraic and topological argument that underpins those assertions, demonstrating that (i) nontrivial topology forces discrete holonomy sectors, (ii) the Lorentz algebra itself generates closed holonomy loops via boost–rotation noncommutativity, and (iii) compact holonomy implies a proper-time phase rate identified with mass. The dynamical

 doi:10.20944/preprints202602.1803.v2

self-consistency of these configurations—including explicit finite-energy solutions of the coupled Einstein–Dirac system—is established in Section 4.

Appendix B.1. Topological Sectors of Lorentz Holonomy

Let γ be a closed loop in spacetime, and let the Lorentz holonomy around γ be

$$\mathrm{Hol}_\gamma(\omega) = \mathcal{P}\exp\oint_\gamma \omega \;\in\; \mathrm{SO}(1,3)\,, \tag{A1}$$

as defined in Equation (2.5). Under local Lorentz gauge transformations, $\mathrm{Hol}_\gamma \mapsto \Lambda(p)\,\mathrm{Hol}_\gamma\,\Lambda^{-1}(p)$, so its conjugacy class is gauge-invariant. If γ is contractible, Hol_γ can still be nontrivial whenever curvature is present; however, it lies in the *topologically trivial* class in the sense that it can be continuously deformed to the identity by shrinking γ to a point. If γ is non-contractible (i.e. represents a nontrivial element of $\pi_1(\mathcal{M})$), then the map $\pi_1 \to \mathrm{SO}(1,3)$ defined by $\gamma \mapsto \mathrm{Hol}_\gamma$ can label distinct global sectors up to conjugacy. In compact (elliptic) subsectors this sector label reduces to an integer winding number via periodicity conditions.

This is the standard mechanism by which topology makes gauge structure physical [29]. Applied to the Lorentz group, it means: on a manifold with non-contractible cycles, distinct winding configurations of the $\mathfrak{so}(1,3)$ connection are topologically stable. They cannot be unwound to the vacuum ($\mathrm{Hol}_\gamma = \mathbb{1}$) by any smooth process.

Appendix B.2. Boosts Generate Rotations: The Algebraic Seed of Winding Closure

The Lorentz algebra $\mathfrak{so}(1,3)$ has six generators: three rotations J_i and three boosts K_i (Equation (2.9)). Their commutation relations include

$$[J_i,\, J_j] = \epsilon_{ijk}\,J_k\,, \quad [J_i,\, K_j] = \epsilon_{ijk}\,K_k\,, \quad [K_i,\, K_j] = -\epsilon_{ijk}\,J_k\,. \tag{A2}$$

The third relation is the crucial one: *two boosts in different directions generate a rotation*. This is the infinitesimal statement of the Wigner–Thomas rotation [5].

At the group level, the finite-element consequence is exhibited by the group commutator of two non-collinear boosts. Consider

$$\Omega(\alpha,\beta) \;=\; e^{\alpha K_x}\,e^{\beta K_y}\,e^{-\alpha K_x}\,e^{-\beta K_y}\,. \tag{A3}$$

This is a closed path in $\mathrm{SO}(1,3)$: it starts and ends at the identity. Applying the Baker–Campbell–Hausdorff formula to leading order:

$$\Omega(\alpha,\beta) \;=\; \exp\!\big(\alpha\beta\,[K_x,K_y] + \mathcal{O}(\alpha^2\beta,\alpha\beta^2)\big) \;=\; \exp\!\big(-\alpha\beta\,J_z + \cdots\big)\,. \tag{A4}$$

Two boosts along x and y, composed as a closed sequence, produce a net rotation about z. The $\mathfrak{so}(1,3)$ algebra thus has an intrinsic loop-closure mechanism: any pair of non-collinear boost generators produces a rotation through their commutator. Winding is not an external imposition on the connection—it is a structural consequence of the algebra's non-abelian character.

Appendix B.3. Closed Holonomy Implies Oscillation

The conjugacy classes of $\mathrm{SO}(1,3)$ include elliptic (rotation-like, eigenvalues $e^{\pm i\vartheta}$), hyperbolic (boost-like, eigenvalues $e^{\pm\phi}$), and parabolic (degenerate/null) elements [5]. The oscillatory confined sectors relevant for particle states correspond to elliptic holonomy classes, since only these belong to compact subgroups and therefore admit periodic internal evolution in proper time.

 doi:10.20944/preprints202602.1803.v2

To make the "self-animation" statement (Section 3.2) precise, consider a field $\Psi(\tau)$ carrying a representation of $\mathrm{Spin}(1,3)$, transported along a timelike worldline with four-velocity $u^\mu = dx^\mu/d\tau$. Parallel transport gives

$$\frac{d\Psi}{d\tau} = -\frac{1}{2}\, u^\mu\, \omega_\mu{}^{ab}\, \Sigma_{ab}\, \Psi\,, \qquad \Sigma_{ab} \equiv \tfrac{1}{4}[\gamma_a, \gamma_b]\,, \tag{A5}$$

so the instantaneous internal generator is the bivector

$$\Xi(\tau) \;\equiv\; \frac{1}{2}\, u^\mu\, \omega_\mu{}^{ab}\, \Sigma_{ab}\,. \tag{A6}$$

If the configuration is approximately stationary in the comoving frame so that $\Xi(\tau) \approx \Xi_0$, then

$$\Psi(\tau) \;\approx\; \exp(-\Xi_0\, \tau)\, \Psi(0)\,. \tag{A7}$$

When Ξ_0 lies in an elliptic conjugacy class, $\exp(-\Xi_0\,\tau)$ is periodic (up to the representation's 2π or 4π identification), and $\Psi(\tau)$ cycles with a well-defined proper-time period T determined by the eigenvalues of Ξ_0. A confined holonomy sector with an elliptic internal generator thus produces periodic proper-time evolution *without an external clock*, because the same connection that defines the sector also defines the transport law (A5).

Appendix B.4. Confinement Scale Determines Mass

The spin connection has dimension $[\omega] \sim 1/\text{length}$. The generator Ξ defined in Equation (A6) therefore has dimension $1/\text{time}$ along a timelike worldline and defines an intrinsic frequency scale. For a confined configuration localized to a characteristic length L, the only natural magnitude for the connection is

$$|\omega| \;\sim\; \frac{1}{L} \qquad\Longrightarrow\qquad |\Xi| \;\sim\; c\,|\omega| \;\sim\; \frac{c}{L}\,. \tag{A8}$$

If the internal evolution is periodic with angular frequency $\omega_{\mathrm{int}} \sim |\Xi|$, then $\omega_{\mathrm{int}} \sim c/L$. On the other hand, a massive degree of freedom has a distinguished proper-time phase rate (Section 3.2):

$$\omega_C \;=\; \frac{mc^2}{\hbar}\,. \tag{A9}$$

Identifying the intrinsic cycling rate of the confined holonomy sector with the Compton rate yields

$$\omega_{\mathrm{int}} \sim \omega_C \qquad\Longrightarrow\qquad \frac{c}{L} \;\sim\; \frac{mc^2}{\hbar} \qquad\Longrightarrow\qquad m \;\sim\; \frac{\hbar}{c\,L}\,, \tag{A10}$$

i.e. the confinement length is the reduced Compton scale $L \sim \bar{\lambda}_C = \hbar/(mc)$, up to $\mathcal{O}(2\pi)$ factors depending on the precise periodicity condition in the chosen representation.

Equation (A10) is the precise sense in which "confinement scale is mass" in the holonomic reading: a stable confined holonomy sector with characteristic size L necessarily introduces a proper-time cycling rate $\sim c/L$, which is the only available invariant that an interior observer can operationally identify as a mass scale. This identification is dimensional: it follows from the only available scales ($\hbar$, c, and L) rather than from a detailed dynamical derivation of the phase evolution in a specific background. The Einstein–Dirac soliton construction of Section 4 provides dynamical self-consistency (the winding can source its own confinement), but the precise numerical coefficient relating ω_{int} to the particle mass depends on the solution branch and has not been computed here.

Appendix B.5. From Confined Holonomy to Curvature Sourcing

The main text uses the chain

$$\text{confined holonomy} \;\Rightarrow\; \text{curvature concentration} \;\Rightarrow\; \nabla \ln \alpha \neq 0 \;\Rightarrow\; \text{mass/weight}\,.$$

 doi:10.20944/preprints202602.1803.v2

This appendix supplies the algebraic content of the first implication: noncommutativity of boosts and rotations produces closed holonomy loops, nontrivial topology makes them topologically stable, and confinement introduces an invariant frequency scale identified with mass. The dynamical realization—explicit finite-energy solutions of the coupled Einstein–Dirac system that realize such nontrivial holonomy sectors—is constructed in Section 4. The cosmological derivations of Sections 5–7 do not require the detailed soliton construction; they require only that persistent matter sources exist satisfying the usual energy conditions, so that null focusing is present and the screen-area monotonicity applies.

References

1. R. Arnowitt, S. Deser, and C. W. Misner, "The dynamics of general relativity," *Phys. Rev.* **116**, 1322–1330 (1959).
2. T. W. Baumgarte and S. L. Shapiro, *Numerical Relativity: Solving Einstein's Equations on the Computer* (Cambridge University Press, 2010).
3. R. S. Phillips, "Anisotropic semi-Dirac inertial mass: The spatial encoding hypothesis," *IPI Letters* **3**(3) (2025).
4. R. S. Phillips, "Geometric origin of the muon anomaly: Predicting the $g-2$ shift via spatial encoding," *IPI Letters* **3**(4) (2025).
5. C. W. Misner, K. S. Thorne, and J. A. Wheeler, *Gravitation* (W. H. Freeman, 1973).
6. R. M. Wald, *General Relativity* (University of Chicago Press, 1984).
7. S. M. Carroll, *Spacetime and Geometry: An Introduction to General Relativity* (Addison-Wesley, 2004).
8. E. Poisson, *A Relativist's Toolkit: The Mathematics of Black-Hole Mechanics* (Cambridge University Press, 2004).
9. A. J. S. Hamilton and J. P. Lisle, "The river model of black holes," *Am. J. Phys.* **76**, 519–532 (2008).
10. P. Painlevé, "La mécanique classique et la théorie de la relativité," *C. R. Acad. Sci. (Paris)* **173**, 677–680 (1921).
11. J. M. Maldacena, "The large N limit of superconformal field theories and supergravity," *Adv. Theor. Math. Phys.* **2**, 231–252 (1998).
12. B. Carter, "Global structure of the Kerr family of gravitational fields," *Phys. Rev.* **174**, 1559–1571 (1968).
13. T. Buchert, "On average properties of inhomogeneous fluids in general relativity: dust cosmologies," *Gen. Relativ. Gravit.* **32**, 105–126 (2000).
14. D. L. Wiltshire, "Cosmic clocks, cosmic variance and cosmic averages," *New J. Phys.* **9**, 377 (2007).
15. D. L. Wiltshire, "Average observational quantities in the timescape cosmology," *Phys. Rev. D* **80**, 123512 (2009).
16. P. R. Smale and D. L. Wiltshire, "Supernova tests of the timescape cosmology," *Mon. Not. R. Astron. Soc.* **413**, 367–385 (2011).
17. J. A. G. Duley, M. A. Nazer, and D. L. Wiltshire, "Timescape cosmology with radiation fluid," *Class. Quantum Grav.* **30**, 175006 (2013).
18. D. L. Wiltshire, "Solution to the cosmological constant problem," arXiv:2404.02129 (2024).
19. C. Clarkson, G. Ellis, J. Larena, and O. Umeh, "Does the growth of structure affect our dynamical models of the Universe? The averaging, backreaction, and fitting problems in cosmology," *Rep. Prog. Phys.* **74**, 112901 (2011).
20. S. R. Green and R. M. Wald, "A new framework for analyzing the effects of small scale inhomogeneities in cosmology," *Phys. Rev. D* **83**, 084020 (2011); arXiv:1011.4920 [gr-qc].
21. A. Sandage, "The change of redshift and apparent luminosity of galaxies due to the deceleration of selected expanding universes," *Astrophys. J.* **136**, 319–333 (1962).
22. A. Loeb, "Direct measurement of cosmological parameters from the cosmic deceleration of extragalactic objects," *Astrophys. J. Lett.* **499**, L111–L114 (1998).
23. J. Liske *et al.*, "Cosmic dynamics in the era of extremely large telescopes," *Mon. Not. R. Astron. Soc.* **386**, 1192–1218 (2008).
24. J. G. Williamson and M. B. van der Mark, "Is the electron a photon with toroidal topology?" *Ann. Fond. Louis de Broglie* **22**(2), 133–160 (1997).
25. L. Susskind, "Computational complexity and black hole horizons," *Fortschr. Phys.* **64**, 24–43 (2016); arXiv:1402.5674 [hep-th].
26. A. R. Brown, D. A. Roberts, L. Susskind, B. Swingle, and Y. Zhao, "Complexity, action, and black holes," *Phys. Rev. D* **93**, 086006 (2016).
27. R. Bousso and N. Engelhardt, "New area law and gravitational thermodynamics," *Phys. Rev. Lett.* **115**, 081301 (2015); arXiv:1504.07627 [hep-th].

 doi:10.20944/preprints202602.1803.v2

28. R. Bousso and N. Engelhardt, "Proof of a new area law in general relativity," *Phys. Rev. D* **92**, 044031 (2015); arXiv:1504.07660 [gr-qc].
29. M. Nakahara, *Geometry, Topology and Physics*, 2nd ed. (CRC Press, 2003).
30. F. Finster, J. Smoller, and S.-T. Yau, "Particle-like solutions of the Einstein–Dirac equations," *Phys. Rev. D* **59**, 104020 (1999); gr-qc/9801079.
31. F. Finster, J. Smoller, and S.-T. Yau, "Particle-like solutions of the Einstein–Dirac–Maxwell equations," *Phys. Lett. A* **259**, 431–436 (1999); gr-qc/9802012.